Anusandhanvallari
Vol 2024, No.1
January 2024
ISSN 2229-3388

Hafnium-Based Magnetic UiO-66 Metal-Organic Framework Nanocomposites; Microwave-Assisted Synthesis and Comprehensive Characterization

[a,b]Mr. S. P. Gawali, [c,d]Dr. Prof. D.V. Mane

[a]Department of Chemistry, Sundarrao More Arts, Commerce and Science College, Poladpur, Raigad, 402303 India

[b]School of Science, Yashwantrao Chavan Maharashtra open University, Nashik, Maharashtra 402222 India

[c]Former, Regional Director, YCMOU Nashik 402222 India

[d]Department of Chemistry, Shri Chhatrapati Shivaji College Omerga, Dharashiv 413606 India

Abstract

This study describes the synthesis and characterization of hafnium-based magnetic metal-organic frameworks (Hf-MMOFs) that combine superparamagnetic behavior with tunable surface functionality. Magnetic Fe_3O_4 nanoparticles were synthesized via microwave-assisted co-precipitation, followed by silica encapsulation and solvothermal growth of functionalized Hf-UiO-66 shells to form Fe_3O_4@SiO_2@Hf-UiO-66 core-shell nanocomposites. Surface modification with carboxylic acid, was achieved through a controlled layer-by-layer approach. Structural, morphological, and magnetic properties were evaluated using XRD, FTIR, SEM, TEM, EDS, and VSM analyses, confirming successful MOF coating, retained crystallinity, and strong magnetic responsiveness. The nanocomposites exhibited saturation magnetization values of 23-41 emu/g, enabling rapid magnetic separation within 30 seconds. Optimal synthesis conditions were identified at 700 W microwave power and 8-9 minutes reaction time, yielding 85-88% conversion. The high stability of Hf-O bonds provides enhanced resistance to hydrolysis and thermal degradation, highlighting their potential for catalytic and environmental applications.

Keywords: Hafnium-based metal-organic frameworks; Magnetic nanocomposites; UiO-66; Microwave-assisted synthesis; Core-shell nanoparticles

1 Introduction

Metal-organic frameworks (MOFs) have emerged as a transformative class of crystalline porous materials, distinguished by their exceptional surface areas, highly tunable architectures, and versatile functional properties [1]. These hybrid materials, constructed from metal ions or clusters coordinated with organic linkers, offer unprecedented control over pore size, shape, and chemical environment, making them attractive candidates for diverse applications including gas storage, catalysis, drug delivery, and sensing [2,3]. Among the extensive library of MOF structures, the UiO-66 topology has garnered particular attention due to its remarkable thermal and chemical stability, which stems from the strong metal-oxygen bonds in its twelve-connected $Zr_6O_4(OH)_4$ clusters. While zirconium-based UiO-66 has been extensively studied and well-characterized, recent research has explored hafnium as an alternative metal center. Hafnium, being in the same group as zirconium, shares similar coordination chemistry but offers distinct advantages, including enhanced Lewis acidity, greater

resistance to hydrolysis, and potentially superior catalytic performance in specific reactions. The incorporation of hafnium into the UiO-66 framework presents exciting opportunities to fine-tune material properties while maintaining the desirable structural features of the parent topology [3-5]. The development of magnetic metal-organic frameworks (MMOFs) represents an innovative advancement that addresses critical challenges in MOF applications, particularly regarding material recovery and recyclability. By integrating magnetic nanoparticles within MOF structures, these composite materials enable facile separation from reaction media using external magnetic fields, thereby eliminating costly and time-consuming filtration or centrifugation steps [6]. This magnetic functionality does not compromise the inherent porosity and surface chemistry of the framework, allowing the material to retain its functional capabilities while gaining practical advantages for industrial-scale implementation. This chapter presents a systematic investigation into the synthesis and comprehensive characterization of hafnium-based magnetic UiO-66 frameworks, exploring various functional groups and employing strategic layer-by-layer approaches to develop advanced composite materials with enhanced properties and practical applicability.

2 Materials and Methods

All chemicals used were of analytical grade and employed without further purification. $FeCl_3 \cdot 6H_2O$ and $FeCl_2 \cdot 4H_2O$ were used for magnetite synthesis, with NH_4OH (28-30%) as the precipitating agent. TEOS served as the silica source. $HfCl_4$ was used as the metal precursor for MOF synthesis, while terephthalic acid, 2-aminoterephthalic acid, and 5-sulfoisophthalic acid monosodium salt were employed as organic linkers. DMF was used as the solvothermal solvent, with acetic acid as a modulator. Ethanol and deionized water were used for washing.

3 Experimental Procedures

3.1 Synthesis of Magnetic Fe_3O_4 Nanoparticles

The synthesis of magnetic magnetite (Fe_3O_4) nanoparticles uses chemical co-precipitation slitly modified [7,8], Involving precipitation of ferric (Fe^{3+}) and ferrous (Fe^{2+}) ions from aqueous solution. The process dissolves iron(III) chloride hexahydrate ($FeCl_3 \cdot 6H_2O$) and iron(II) chloride tetrahydrate ($FeCl_2 \cdot 4H_2O$) in deionized water at a 2:1 molar ratio in deionized water. The synthesis proceeded through the following stoichiometric reaction .

$$Fe^{3+} + 2Fe^{2+} + 8OH^- \rightarrow Fe_3O_4 + 4H_2O. \quad (1)$$

The system is deoxygenated by purging with nitrogen (N_2) gas for 15 minutes while heated in an 80 ^{0}C oil bath. The precipitation reaction begins with dropwise addition of ammonium hydroxide (NH_4OH) under stirring, increasing pH to form magnetite, changing color from yellow-brown to black. The overall chemical reaction can be represented as:

$$2FeCl_3 + FeCl_2 + 8NH_4OH \rightarrow Fe_3O_{4(s)} + 8NH_4Cl_{(aq)} + 4H_2O_{(l)} \quad (2)$$

The fundamental chemical transformation occurring during this process can be represented by the equation:

$$Fe^{2+} + 2Fe^{3+} + 8OH^- \rightarrow Fe_3O_4 + 4H_2O \quad (3)$$

After precipitation, the slurry is subjected to microwave irradiation to promote the crystallization and growth of the nanoparticles [9, 10].

Anusandhanvallari
Vol 2024, No.1
January 2024
ISSN 2229-3388

3.2 Synthesis of Fe_3O_4@SiO_2 Core-Shell Nanoparticles

Fe3O4@SiO2 core-shell nanoparticles were synthesized using a modified Stöber method with microwave heating. Nanoparticles were dispersed in water-ethanol mixture and ultrasonicated. The pH was adjusted to 11 using NaOH, followed by sodium metasilicate addition under stirring and microwave heating. The pH was reduced to 9 using HCl to form a uniform SiO2 shell as shown in Figure 1. The silica coating prevents agglomeration and enhances magnetic nanoparticle stability [11].

The core-shell product is washed with deionized water until neutral pH, followed by ethanol. The nanoparticles are collected using an external magnet and dried to yield a fine powder.

$$Na_2SiO_3(aq) + 3H_2O(l) \xrightarrow{Base\ catalyst} Si(OH)_4\ (aq) + 2NaOH\ (aq) \quad (4)$$

$$nSi(OH)_4\ (aq) \xrightarrow{Condensation on\ Fe3O4\ surface} (SiO_2)_n(s) + 2n\ H_2O\ (l) \quad (5)$$

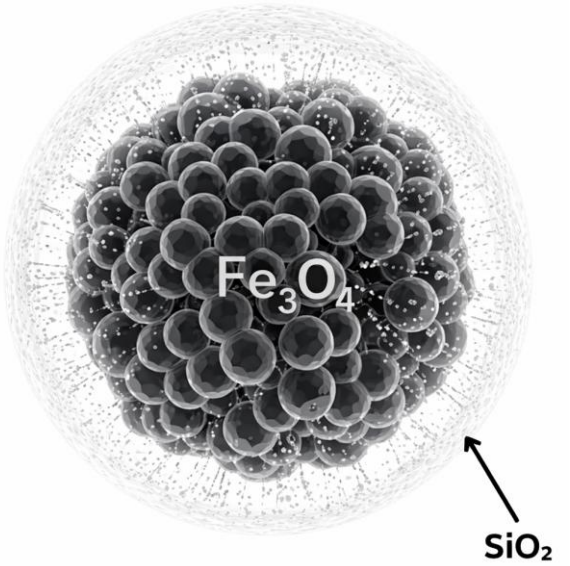

Figure 3 Core-shell structural model of Fe_3O_4@SiO_2 nanoparticles showing Fe_3O_4 magnetic core encapsulated within the SiO_2 shell.

3.3 Synthesis of Hf-UiO-66 (HF01)

Hf-UiO-66 (HF01) was synthesized via a microwave-assisted solvothermal method using $HfCl_4$ as the metal source and 1,4-benzenedicarboxylic acid (H_2BDC) as the organic linker. The reaction was carried out in DMF with HCl as a modulator to control crystal growth and enhance crystallinity. Microwave heating at 80 °C and 700 W enabled rapid formation of the $Hf_6O_4(OH)_4(BDC)_6$ secondary building units, yielding a highly ordered UiO-66 framework [12]. The resulting MOF exhibits a face-centered cubic structure with characteristic octahedral cages as shown in **Figure 2**.

Anusandhanvallari
Vol 2024, No.1
January 2024
ISSN 2229-3388

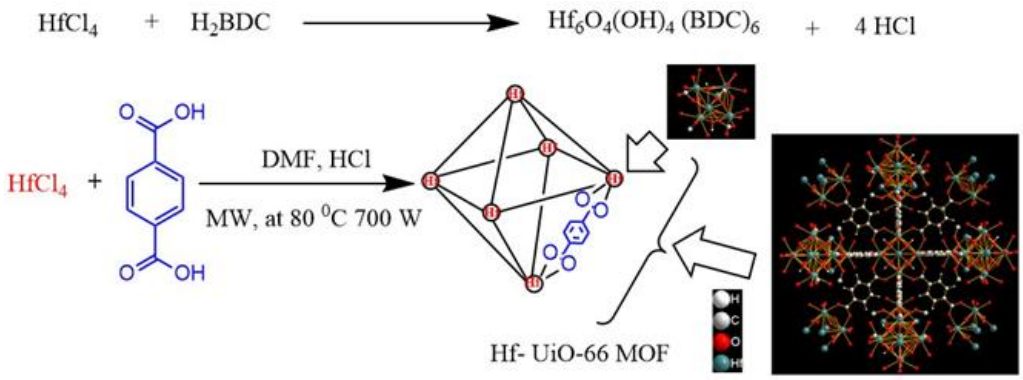

Figure 2 Microwave-assisted synthesis of Hf-UiO-66 MOF using $HfCl_4$ and H_2BDC in DMF/HCl, showing cluster formation of $Hf_6O_4(OH)_4(BDC)_6$ and the resulting 3D framework.

3.4 Synthesis of Hf-MMOF-1 (Fe_3O_4@SiO_2-Hf-UiO-66)

The synthesis of Hf-MMOF-1 begins by dispersing 1.0 g of Fe_3O_4@SiO_2 in 45 mL DMF and ultrasonicating for 30 minutes. The MOF forms through terephthalic acid linker coordination to hafnium metal centers [13, 14], where hexanuclear hafnium-oxo clusters connect with twelve carboxylate linkers to form the framework. $HfCl_4$ (2 mmol, 0.5567 g) is added with 10 minutes ultrasonication, followed by Terephthalic Acid acid H_2BDC (2 mmol, 0.332 g) dissolved in 10 mL DMF and 0.9 mL HCl. The mixture is microwave-heated at 80 ^{0}C for 8 minutes at 700 W, then reacted for 12 hours. The product is washed with DMF for 12 hours and dried at 50°C for 24 hours. See Figure 3

$$HfCl_4 + H_2BDC \rightarrow Hf_6O_4(OH)_4(BDC)_6 + 4HCl \quad (6)$$

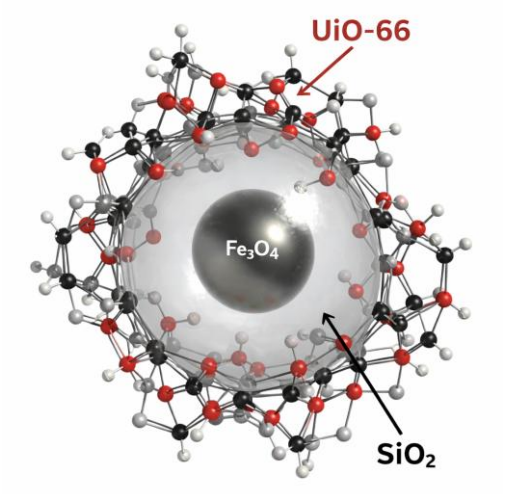

Figure 3. Fe3O4@SiO2 -UiO-66 (Hf) shell nanocomposite depicting the magnetic Fe_3O_4 core, SiO_2 interlayer, and UiO-66 metal-organic framework shell.

4 Results and Discussion

4.1 X-ray Diffraction (XRD) Analysis

XRD recorded on Panalytical's X'Pert Pro, which is indispensable for confirming the crystalline structure, phase purity, and lattice parameters of the synthesized MOFs and their magnetic components. As shown in **Figure 4** allows for the identification of the characteristic diffraction patterns of Fe_3O_4, SiO_2, and the UiO-66 framework, and can reveal structural changes due to defect engineering. These XRD patterns demonstrate the crystalline structure evolution during the stepwise functionalization of Fe_3O_4 magnetic nanoparticles with silica coating and UiO-66 MOF variants [15, 16]. The base Fe_3O_4 nanoparticles exhibit the characteristic cubic spinel structure with well-defined diffraction peaks at 2θ values of approximately 30.1° (220), 35.5° (311), 43.1° (400), 57.0° (511), and 62.6° (440), which correspond to the standard magnetite phase and confirm the successful synthesis of crystalline magnetic nanoparticles. Prominent diffraction peaks indexed match well with standard JCPDS data for Fe_3O_4 as in **Table 1-3**.

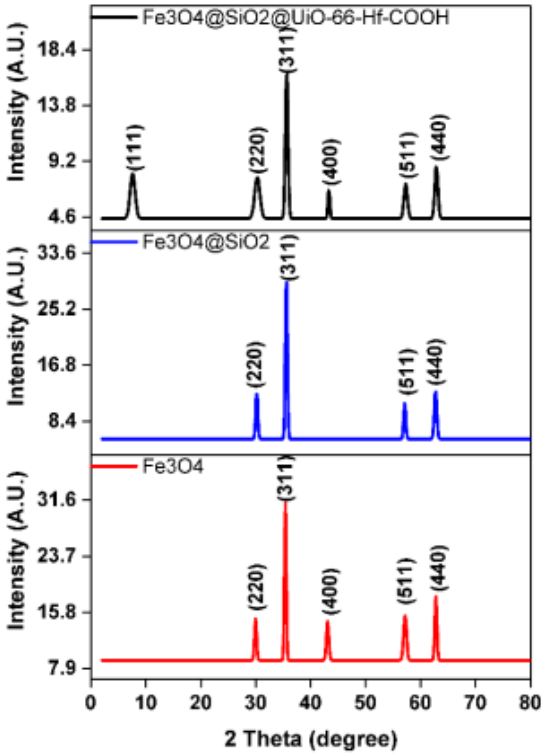

Figure 4 XRD patterns of a) Fe_3O_4 b) Fe_3O_4@SiO_2 c) UiO-66 (Hf) and d) Fe_3O_4@SiO_2 -UiO-66 (Hf)

After silica coating, these peaks were retained with slight intensity reduction, indicating an amorphous SiO_2 shell without disrupting the magnetic core. Upon UiO-66 functionalization, the Fe_3O_4 peaks remained prominent, demonstrating preserved core crystallinity, while the appearance of a low-angle reflection at 11-12° confirmed the formation of the UiO-66 framework [17, 18]. Minor peak shifts and reduced crystallite sizes suggest surface interactions and suppressed grain growth after coating. The absence of impurity phases confirms the successful synthesis of phase-pure, structurally stable magnetic MOF nanocomposites [19].

Table 1 X-ray diffraction (XRD) data for Fe_3O_4 nanoparticles, including Miller indices (hkl), diffraction angles (2θ, θ), interplanar spacing (d), lattice parameter (a), and crystallite size (D)

Fe_3O_4										
h	k	l	2θ	θ	Sinθ	2Sinθ	d	$(a/d)^2$	a	D nm
2	2	0	29.961	14.981	0.259	0.517	2.979	7.912	8.426	18.17
3	1	1	35.367	17.683	0.304	0.608	2.535	10.926	8.409	22.38
4	0	0	43.089	21.544	0.367	0.735	2.097	15.968	8.388	16.17
5	1	1	53.900	26.950	0.453	0.907	1.699	24.321	8.829	14.88
4	4	0	57.181	28.591	0.479	0.957	1.609	27.117	9.103	14.50
									8.631	**17.222**

Table 2 X-ray diffraction (XRD) data for Fe_3O_4@SiO_2, including Miller indices (hkl), diffraction angles (2θ, θ), interplanar spacing (d), lattice parameter (a), and crystallite size (D)

$Fe_3O_4@SiO2$										
h	k	l	2θ	θ	Sinθ	2Sinθ	d	$(a/d)^2$	a	D nm
2	2	0	30.183	15.092	0.260	0.521	2.958	8.027	8.366	18.520
3	1	1	35.565	17.782	0.305	0.611	2.522	11.044	8.363	19.859
4	0	0	43.476	21.738	0.370	0.741	2.079	16.242	8.317	20.232
5	1	1	57.128	28.564	0.478	0.956	1.611	27.070	8.369	20.221
4	4	0	62.735	31.367	0.521	1.041	1.479	32.082	8.369	17.048
									8.357	**19.176**

Table 3 X-ray diffraction (XRD) data for Hf-MMOF-1 including Miller indices (hkl), diffraction angles (2θ, θ), interplanar spacing (d), lattice parameter (a), and crystallite size (D)

Hf-MMOF-1 ($Fe^3O^4@SiO^2@UiO-66(Hf)$)										
h	k	l	2θ	θ	Sinθ	2Sinθ	d	$(a/d)^2$	a	D nm
1	1	1	7.592	3.796	0.066	0.132	11.632	0.519	20.146	7.538
2	2	0	30.280	15.140	0.261	0.522	2.949	8.077	8.340	7.377
3	1	1	35.626	17.813	0.306	0.612	2.517	11.081	8.349	15.075
4	0	0	43.327	21.664	0.369	0.738	2.086	16.137	8.344	21.023
5	1	1	57.304	28.652	0.480	0.959	1.606	27.224	8.345	12.180
4	4	0	62.87636	31.438	0.522	1.043	1.477	32.212	8.352	13.796
									10.313	**12.831**

4.2 Fourier Transform Infrared Spectroscopy (FTIR):

FTIR spectra were recorded at SAIF, Panjab University, using a PerkinElmer Spectrum RX FTIR to identify functional groups and confirm stepwise surface modification. Bare Fe_3O_4 nanoparticles exhibited characteristic Fe-O stretching vibrations at 533-461 cm^{-1}, confirming the formation of the magnetic core. After silica coating, the appearance of Si-O stretching bands around 1022-1034 cm^{-1} verified successful SiO_2 encapsulation without affecting the Fe_3O_4 core. Subsequent functionalization with UiO-66 variants introduced characteristic organic linker vibrations, including C=O and C-H stretching bands, confirming MOF growth and functional group incorporation. The consistent presence of Fe-O bands across all samples indicates preserved magnetic integrity, demonstrating successful synthesis of multifunctional magnetic MOF composites. as shown in **Figure 5** [20-23].

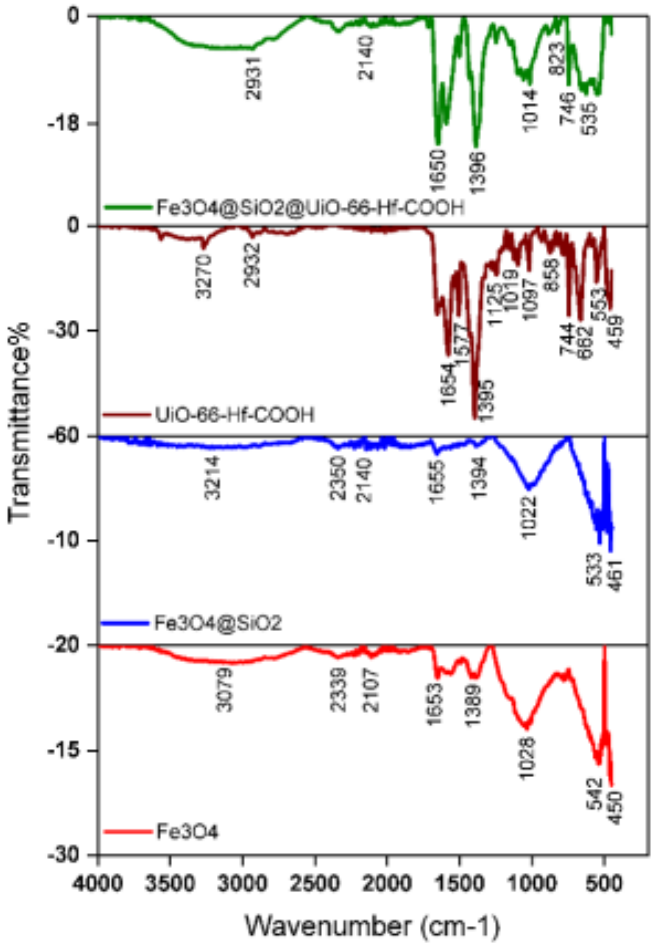

Figure 5. FTIR spectra of a) Fe_3O_4 b) Fe_3O_4@SiO_2 c) UiO-66 (Hf) and d) Fe_3O_4@SiO_2 -UiO-66 (Hf)

4.3 Scanning Electron Microscopy (SEM):

SEM analysis was carried out at DST-SAIF Cochin using a JEOL 6390LA microscope to examine surface morphology and particle size. Pristine Fe_3O_4 nanoparticles exhibited uniform spherical morphology with smooth

surfaces. After silica coating, the Fe_3O_4@SiO_2 particles retained their spherical shape with increased surface roughness and size, confirming shell formation [24]. UiO-66-Hf MOFs displayed characteristic octahedral crystals with well-defined facets, while functional groups influenced crystal size without altering the overall geometry. The Fe_3O_4@SiO_2@UiO-66-Hf composites showed successful core-shell integration, with octahedral MOF crystals anchored onto spherical magnetic cores, confirming the formation of hybrid magnetic MOF structures as shown in **Figure 6** [25].

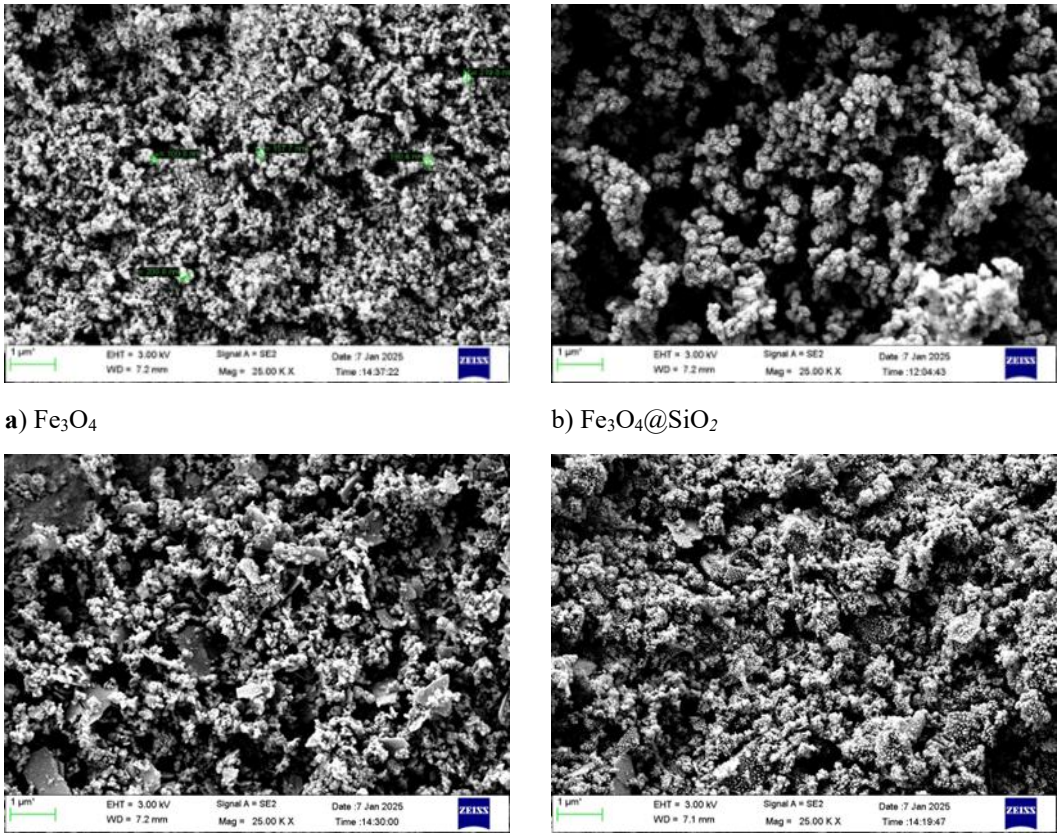

a) Fe_3O_4 b) Fe_3O_4@SiO_2

c) UiO-66 (Hf) d) Fe_3O_4@SiO_2 -UiO-66 (Hf)

Figure 6. SEM images of a) Fe_3O_4 b) Fe_3O_4@SiO_2 c) UiO-66 (Hf) and d) Fe_3O_4@SiO_2 -UiO-66 (Hf)

4.4 Elemental Analysis (EDX)

EDS analysis at DST-SAIF Cochin (JEOL 6390LA/OXFORD XMX N) provided elemental composition (C, H, N, S, Hf, Fe, Si) of the synthesized materials, confirming successful functionalization. Pristine Fe_3O_4 nanoparticles showed characteristic Fe and O peaks, verifying magnetite formation. Silica-coated Fe_3O_4@SiO_2 displayed additional Si and O peaks, indicating shell deposition without disrupting the Fe_3O_4 core. UiO-66-Hf MOFs exhibited Hf, C, and O peaks, with variations reflecting different functional groups, such as enhanced C and O signals in UiO-66 (Hf) from carboxyl incorporation [26] as shown in **Figure 7**.

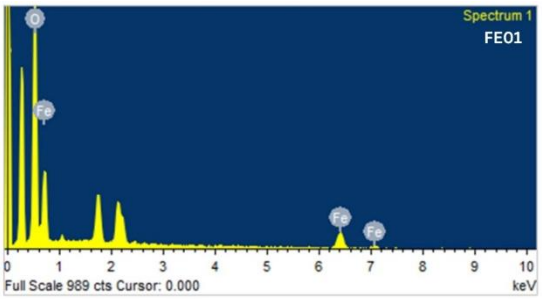

a) Fe_3O_4

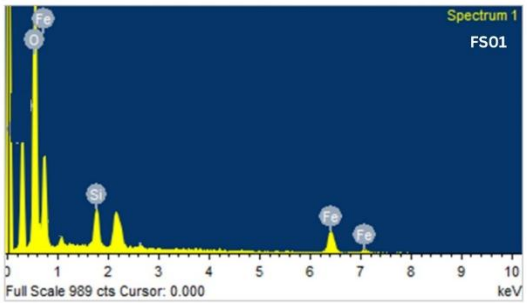

b) Fe_3O_4@SiO_2

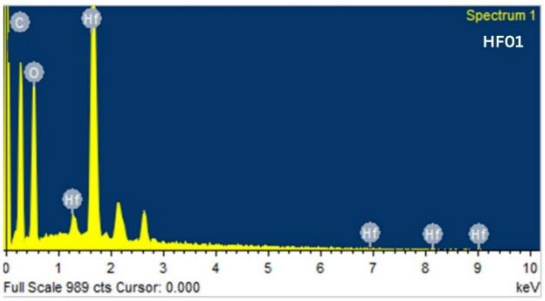

c) UiO-66 (Hf)

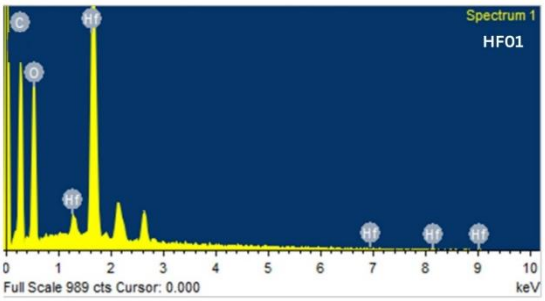

d) Fe_3O_4@SiO_2 -UiO-66 (Hf)

Figure 7 EDX pattern of a) Fe_3O_4 b) Fe_3O_4@SiO_2 c) UiO-66 (Hf) and d) Fe_3O_4@SiO_2 -UiO-66 (Hf)

The composite materials Fe3O4@SiO2 -UiO-66 (Hf) series demonstrate the coexistence of all constituent elements, with Fe and Si peaks from the magnetic core and silica shell, along with Hf, C, O, from the MOF coating, confirming the successful assembly of the hierarchical core-shell-MOF architecture [27-28].

4.5 Transmission Electron Microscopy (TEM):

TEM TEM analysis at SAIF Mumbai provided high-resolution imaging of the synthesized nanoparticles and composites, revealing detailed morphology, size, and core-shell structures. Fe_3O_4 nanoparticles were uniform and spherical (10-15 nm) with SAED patterns confirming their cubic spinel crystallinity. Silica-coated Fe_3O_4@SiO_2 displayed a clear core-shell structure, with a dark Fe_3O_4 core surrounded by an amorphous SiO_2 shell, as indicated by SAED (**Figure 8**). UiO-66-Hf MOF derivatives (**Figure 8**) are expected to be crystalline nanoparticles with well-defined shapes, verified by TEM and SAED. The Fe_3O_4@SiO_2@UiO-66-Hf composites exhibited a three-layer architecture, clearly showing the magnetic core, silica interlayer, and crystalline MOF outer shell [29-30], with SAED patterns reflecting the crystallinity of both the core and the MOF, confirming successful multi-layered assembly as shown in **Figure 8**.

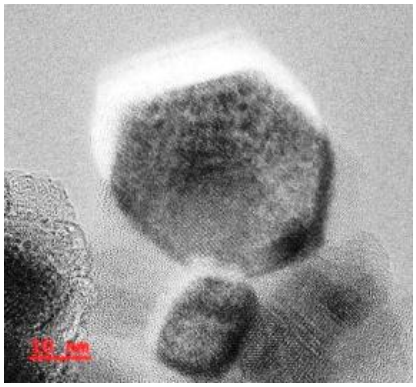

a) Fe_3O_4

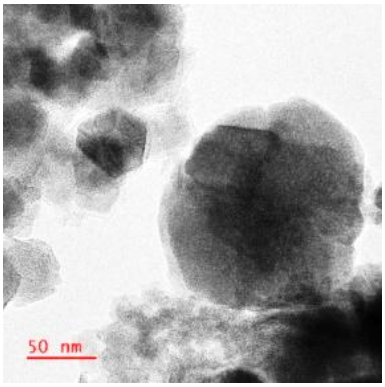

b) $Fe_3O_4@SiO_2$

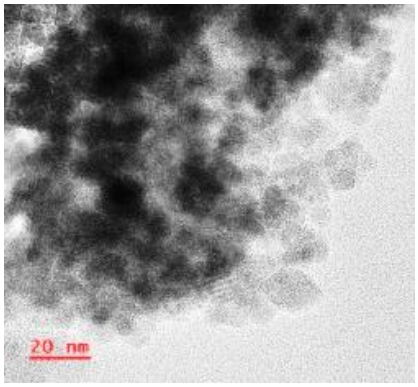

c) UiO-66 (Hf)

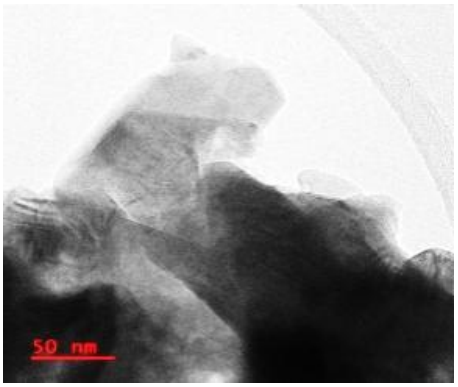

d) $Fe_3O_4@SiO_2$ -UiO-66 (Hf)

Figure 8 HR-TEM of a) Fe_3O_4 b) $Fe_3O_4@SiO_2$ c) UiO-66 (Hf) and d) $Fe_3O_4@SiO_2$ -UiO-66 (Hf)

The bare Fe_3O_4 nanoparticles exhibit a size of 147.5 nm, which slightly increases to 157.7 nm upon SiO_2 coating, indicating successful shell formation. UiO-66-Hf composites display varied sizes the COOH-functionalized version has 230.5 nm,

Table 4 Particle Size (via TEM), zeta potential (mV), and electrophoretic mobility (cm^2/Vs) of various synthesized Fe_3O_4, $Fe_3O_4@SiO_2$ and d) $Fe_3O_4@SiO_2$ -UiO-66 (Hf samples including based frameworks, and their composites.

Sample	Particle size	Zeta Potential	Electrophoretic Mobility
	(nm)	(Mv)	($cm^{2/}Vs$)
Fe_3O_4	147.5	-41.4	-0.000321

Fe_3O_4@SiO_2	157.7	-23.5	-38.4	-0.000182	-0.0003
Fe_3O_4@SiO2-UiO-66(Hf)	230.5	-17		-0.000132	

4.6 Vibrating Sample Magnetograph (VSM):

VSM analysis at SAIF Mumbai evaluated the magnetic properties of the synthesized materials. Fe_3O_4 nanoparticles exhibited superparamagnetism with a saturation magnetization (Ms) of 28 emu/g. Silica-coated Fe_3O_4@SiO_2 retained superparamagnetism with increased Ms (41 emu/g). Pure UiO-66-Hf MOFs were diamagnetic, but when combined with the magnetic cores, the resulting Fe_3O_4@SiO_2@UiO-66-Hf composites remained superparamagnetic, though with reduced Ms (23-30 emu/g) due to the non-magnetic MOF shell. This preserved magnetic responsiveness enables efficient magnetic separation [30-31].

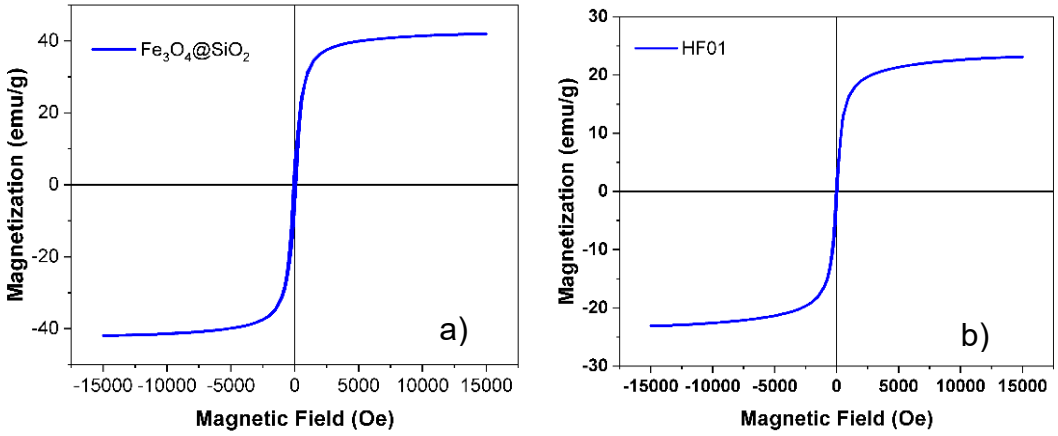

Figure 9. VSM images of a) Fe_3O_4@SiO_2 and b) Fe_3O_4@SiO_2 -UiO-66 (Hf)

4.7 Stability and Reusability:

Hf-based UiO-66 frameworks combine exceptional chemical and thermal stability with practical magnetic recoverability. Strong Hf-O bonds (~790 kJ/mol) confer resistance to hydrolysis, acids, and high temperatures, while superparamagnetic Fe_3O_4 cores enable easy separation and recycling without aggregation, maintaining performance over multiple cycles. Comprehensive characterization confirmed the integrity and functionality of these composites: XRD verified crystalline phase purity of both Fe_3O_4 and UiO-66 components; FTIR confirmed linker coordination and functional group incorporation; SEM/TEM visualized core-shell structures with well-defined octahedral MOF crystals; EDS validated elemental composition including Hf, Fe, Si, and functional heteroatoms; and VSM demonstrated retained superparamagnetism. Together, these results establish that the synthesized Hf-MMOF composites possess robust structural, chemical, and magnetic properties, making them highly suitable for industrial applications requiring stable, reusable catalysts or adsorbents.

5 Conclusion

The successful synthesis and comprehensive characterization of hafnium-based magnetic MOF composites with diverse functional groups. The study established microwave-assisted Fe_3O_4 nanoparticle synthesis, effective silica encapsulation, and solvothermal growth of Hf-UiO-66 derivatives with carboxyl functionalities, producing stable core-shell-shell nanocomposites. Characterization confirmed structural integrity, functionalization, and retention of superparamagnetic behavior, enabling rapid magnetic separation within 30 seconds. These Hf-MMOFs combine chemical robustness, tunable functionality, and practical magnetic recoverability, making them promising candidates for heterogeneous catalysis, adsorption, separation, environmental remediation, and sensing applications. The work provides a clear framework for understanding structure-property relationships in magnetic MOFs and lays the foundation for designing next-generation multifunctional materials, with future studies aimed at optimizing performance through systematic variation of synthesis parameters and application-specific testing.

Reference

[1] Zheng, Y., Pang, H., Xue, H., & Zheng, S.. Metal-Organic Frameworks/Graphene-Based Materials: Preparations and Applications. Advanced Functional Materials, 28(47) (2018), 1804950.

[2] Remya, V. R., & Kurian, M. Synthesis and catalytic applications of metal\u2013organic frameworks: a review on recent literature. International Nano Letters, 9(1), (2018)., 17–29.

[3] He, T., Wang, X., Long, Y., Wang, H., Ni, B., Xu, X., & Hu, W. Fast and scalable synthesis of uniform zirconium-, hafnium-based metal-organic framework nanocrystals. Nanoscale, 9(48), (2017), 19209–19215.

[4] Rimoldi, M., Goswami, S., Lin, L., Howarth, A. J., Li, P., Farha, O. K., Hupp, J. T., & Destefano, M. R. Catalytic Zirconium/Hafnium-Based Metal–Organic Frameworks. ACS Catalysis, 7(2), (2016). 997–1014.

[5] Cirujano, F. G., & Llabrés I Xamena, F. X. Tuning the Catalytic Properties of UiO-66 Metal-Organic Frameworks: From Lewis to Defect-Induced Brønsted Acidity. The Journal of Physical Chemistry Letters, 11(12), (2020). 4879–4890.

[6] Vo, T. K., & Kim, J. (2021). Facile synthesis of magnetic framework composite $MgFe_2O_4$@UiO-66(Zr) and its applications in the adsorption-photocatalytic degradation of tetracycline. Environmental Science and Pollution Research, 28(48), (2021). 68261–68275.

[7] Z. Hu, Y. Wang, D. Zhao, The chemistry and applications of hafnium and cerium (IV) metal–organic frameworks, Chemical Society Reviews, 50 (2021) 4629-4683.

[8] S. Ding, L. Chen, J. Liao, Q. Huo, Q. Wang, G. Tian, W. Yin, Harnessing Hafnium-Based Nanomaterials for Cancer Diagnosis and Therapy, Small, 19 (2023) 2300341.

[9] Y. Wei, B. Han, X. Hu, Y. Lin, X. Wang, X. Deng, Synthesis of Fe_3O_4 nanoparticles and their magnetic properties, Procedia Engineering, 27 (2012) 632-637.

[10] X.-M. Li, G. Xu, Y. Liu, T. He, Magnetic Fe3O4 nanoparticles: synthesis and application in water treatment, Nanoscience & Nanotechnology-Asia, 1 (2011) 14-24.

[12] M.G. Afshara, M. Rajabib, M. Payehghadrb, N.B. Panahb, Fe_3O_4@ SiO_2 Magnetic Core-Shell Nanoparticles Functionalized with 1, 4-dihydroxyanthraquinone as an Effective and Recyclable Adsorbent for Removal of Copper Ion from Aqueous Solutions, DOI (2024).

[13] X.-W. Gu, J. Pei, K. Shao, H.-M. Wen, B. Li, G. Qian, Chemically stable hafnium-based metal–organic framework for highly efficient C_2H_6/C_2H_4 separation under humid conditions, ACS Applied Materials & Interfaces, 13 (2021) 18792-18799.

[14] Y.-X. Wang, R. Wang, Z.-X. Wang, Q. Shen, S. Liu, G. Li, Post-synthetic modification of MOF-808: Innovative strategies, structural and performance regulation, Inorganic Chemistry Frontiers, DOI (2026).

[15] A.R.P. Hidayat, L.L. Zulfa, N. Faaizatunnisa, D. Prasetyoko, D. Hartanto, N. Widiastuti, A.S. Purnomo, M. Jannah, E.N. Kusumawati, R. Ediati, Properties of Ni (II)-doped magnetic Fe3O4@ mesoporous SiO2/Uio-66 synthesized by an ultrasound assisted method for potential adsorbents of methyl orange: kinetic, isotherm and thermodynamic studies, Isotherm and Thermodynamic Studies, DOI.

[16] D. Chicea, E. Indrea, C. Cretu, Assesing Fe_3O_4 nanoparticle size by DLS, XRD and AFM, Journal of optoelectronics and advanced materials, 14 (2012) 460.

[17] H. El Ghandoor, H. Zidan, M.M. Khalil, M. Ismail, Synthesis and some physical properties of magnetite (Fe_3O_4) nanoparticles, International journal of electrochemical science, 7 (2012) 5734-5745.

[18] M. Aghayi-Anaraki, V. Safarifard, Fe_3O_4@ MOF magnetic nanocomposites: Synthesis and applications, European Journal of Inorganic Chemistry, 2020 (2020) 1916-1937.

[19] G. Hootifard, E. Sheikhhosseini, S.A. Ahmadi, M. Yahyazadehfar, Fe_3O_4@ iron-based metal–organic framework nanocomposite [Fe_3O_4@ MOF (Fe) NC] as a recyclable magnetic nano-organocatalyst for the environment-friendly synthesis of pyrano [2, 3-d] pyrimidine derivatives, Frontiers in Chemistry, 11 (2023) 1193080.

[20] F. Babaei, A. Ghasemi, Structural, optical and magnetic properties of nickel–copper ferrite NixCu1− x Fe 2O4, Optical and Quantum Electronics, 54 (2022) 697.

[21] R.M. Cornell, U. Schwertmann, The iron oxides: structure, properties, reactions, occurrences, and uses, Wiley-vch Weinheim 2003.

[22] E. Verwey, E. Heilmann, Physical properties and cation arrangement of oxides with spinel structures I. Cation arrangement in spinels, The Journal of Chemical Physics, 15 (1947) 174-180.

[23] M.E. Fleet, The structure of magnetite, Structural Science, 37 (1981) 917-920.

[24 S. Sajjadifar, I. Amini, M. Karimian, Synthesis and characterization of Fe_3O_4@ APTES@ MOF-199 magnetic nanocatalyst and its application in the synthesis of quinoxaline derivatives, Iranian Journal of Catalysis, 11 (2021).

[25] G. Sargazi, D. Afzali, A.K. Ebrahimi, A. Badoei-Dalfard, S. Malekabadi, Z. Karami, Ultrasound assisted reverse micelle efficient synthesis of new Ta-MOF@ Fe3O4 core/shell nanostructures as a novel candidate for lipase immobilization, Materials Science and Engineering: C, 93 (2018) 768-775.

[26] H. Mahajan, S.K. Godara, A. Srivastava, Synthesis and investigation of structural, morphological, and magnetic properties of the manganese doped cobalt-zinc spinel ferrite, Journal of Alloys and Compounds, 896 (2022) 162966.

[27] H. Lu, L. Zhang, B. Wang, Y. Long, M. Zhang, J. Ma, A. Khan, S.P. Chowdhury, X. Zhou, Y. Ni, Cellulose-supported magnetic Fe_3O_4–MOF composites for enhanced dye removal application, Cellulose, 26 (2019) 4909-4920.

[28] J.I. Goldstein, D.E. Newbury, J.R. Michael, N.W. Ritchie, J.H.J. Scott, D.C. Joy, Scanning electron microscopy and X-ray microanalysis, springer2017.

[29] O. Zaremba, J. Andreo, S. Wuttke, The chemistry behind room temperature synthesis of hafnium and cerium UiO-66 derivatives, Inorganic Chemistry Frontiers, 9 (2022) 5210-5216.

[30] A.G. Roca, L. Gutiérrez, H. Gavilán, M.E.F. Brollo, S. Veintemillas-Verdaguer, M. del Puerto Morales, Design strategies for shape-controlled magnetic iron oxide nanoparticles, Advanced drug delivery reviews, 138 (2019) 68-104.

[31] M. Mahmoudi, S. Sant, B. Wang, S. Laurent, T. Sen, Superparamagnetic iron oxide nanoparticles (SPIONs): development, surface modification and applications in chemotherapy, Advanced drug delivery reviews, 63 (2011) 24-46.